Topology in solid state physics.

Topology is originally a subject of mathematics. It allows us to classify objects according to their geometric structure. However, the objects we are trying to characterize according to its geometric property or topology can appear in many different contexts. Therefore, topological classification applies across many different fields and it is universal tool box to geometrically characterize objects. For example, consider a vector field as shown below:

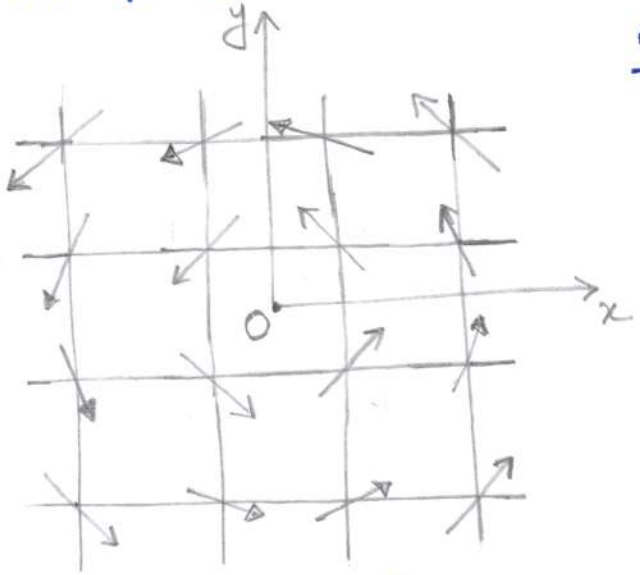

Fig. 1 (a)

In the Cartesian co-ordinate system the vector field can be represented as

$$\vec{F} = \left(-\frac{y}{x^2+y^2} , \frac{x}{x^2+y^2} \right)$$

$$\equiv F_x \hat{i} + F_y \hat{j},$$

where $\hat{i}$ and $\hat{j}$ are unit vectors in the x and y directions. A factor of $1/(x^2+y^2)$ is introduced in the definition of $\vec{F}$ to capture the fact that the vector field rotates about the origin O slowly as we move further away from it. As the vector field circulates around the origin, we can exploit another venerable concept of physics: Symmetry. In the given situation the vector field possesses a circular or cylindrical symmetry in the xy plane

Therefore, it is convenient to express the vector field in the circular or cylindrical co-ordinates, i.e., $\vec{F} = F_r \hat{r} + F_\phi \hat{\phi}$, where $\hat{r}$ and $\hat{\phi}$ are the unit vectors in the radial and azimuthal directions, respectively, and F_r and F_ϕ are the components of the vector $\vec{F}$ in these two directions.

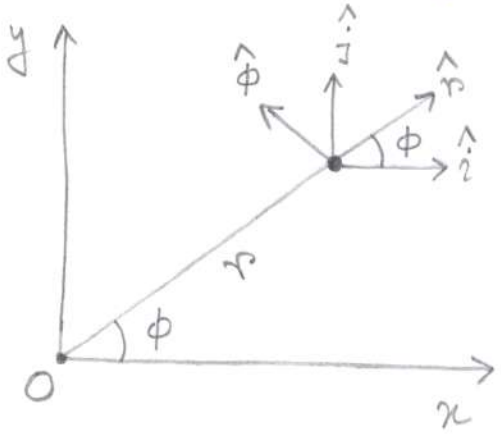

Fig. 2

Identities: $\hat{i}.\hat{r} = \cos\phi$, $\hat{j}.\hat{r} = \sin\phi$

$\hat{i}.\hat{\phi} = -\sin\phi$, $\hat{j}.\hat{\phi} = \cos\phi$.

$$F_r = F_x(\hat{i}.\hat{r}) + F_y(\hat{j}.\hat{r}).$$
$$= F_x\cos\phi + F_y\sin\phi.$$
$$F_\phi = F_x(\hat{i}.\hat{\phi}) + F_y(\hat{j}.\hat{\phi})$$
$$= -F_x\sin\phi + F_y\cos\phi.$$

In circular or cylindrical coordinates, $x = r\cos\phi$ and $F_y = r\sin\phi$, yielding

$F_x = -\frac{\sin\phi}{r}$ and $F_y = \frac{\cos\phi}{r}$, and therefore.

$F_r = -\frac{\sin\phi\cos\phi}{r}$ and $F_\phi = \frac{1}{r}(\sin^2\phi + \cos^2\phi) = \frac{1}{r}$.

$+\frac{\sin\phi\cos\phi}{r} = 0$

Now, we compute the closed line integral around the origin at any fixed radius $r = R$.

$$\oint_C \vec{F}.d\vec{l} = \frac{1}{R}\int_{\phi=0}^{2\pi} R\,d\phi = 2\pi \Rightarrow \boxed{\frac{1}{2\pi}\oint_C \vec{F}.d\vec{l} = 1}$$

The quantity on the right-hand-side counts how many

times the vector field wraps around the origin measured in units of 2π for the sake of normalization. Now consider the following vector field, obtain $-\vec{\omega}$ by "flipping" the direction of all arrows. In this case, the vector field is

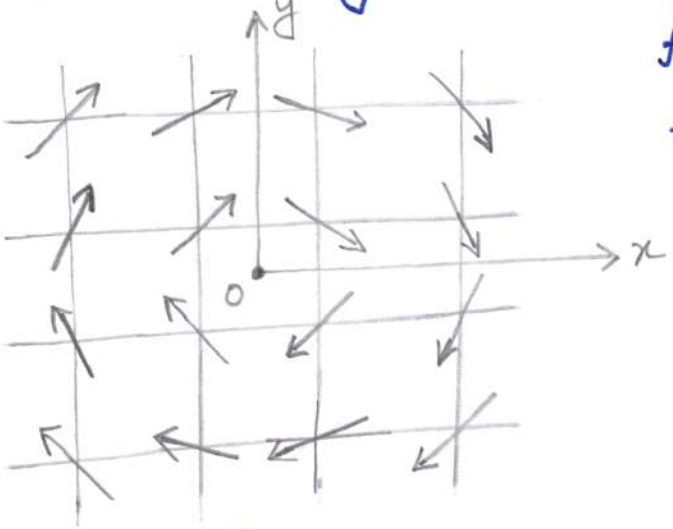

Fig. 1 (b)

$$\vec{F} = -\left(-\frac{y}{x^2+y^2}, \frac{x}{x^2+y^2}\right)$$

$$\Rightarrow \boxed{\frac{1}{2\pi}\oint_c \vec{F}\cdot d\vec{l} = -1}$$

This conclusion directly contradicts the Stoke's theorem, as $\vec{F}$ can be written as

$\vec{F} = \vec{\nabla}\Phi(x,y)$, where $\Phi(x,y)$ is a scalar function, given by $\Phi(x,y) = \tan^{-1}\left(\frac{y}{x}\right)$

Then $\oint_c \vec{F}\cdot d\vec{l} = \oint_c \vec{\nabla}\Phi\cdot d\vec{l} = \int_S \vec{\nabla}\times(\vec{\nabla}\Phi)\cdot d\vec{s} \equiv 0.$

S is the surface enclosed by a closed contour c

How to resolve this paradox?

Note that $\vec{F} = \vec{\nabla}\Phi(x,y)$ is true, everywhere in the space, except at the origin where $r=0$ or $x=y=0$. What we discussed so far correspond to a "vortex" configuration of the vector field in Fig. 1(a) and an "anti-vortex" configuration of the vector field in Fig. 1(b). The origin

corresponds to the "core" of such defects.
Notice that if we want to go from configura-tion 1(a) to 1(b), we have to flip the direction of the vector field at each and every point of space, which is NOT a SMOOTH process. This is a good place to take a brief pause and summarize what we learned so far:

1) Topological defects are characterized by a quanti-ty, which we name topological invariant. In the case we discussed so far the topological invariant is given by

$$N = \frac{1}{2\pi} \oint_C \vec{F} \cdot d\vec{l} = \pm 1 .$$

: vorticity

for the vector field $\vec{F}$. In case of vortex or anti-vortex, the topological invariant N can take any integer value of either sign. Such invariants are called $\mathbb{Z}$ invariants, where $\mathbb{Z}$ is the set of all integers.

2) Topological defects with distinct topological invariants can not be smoothly deformed into each other. In other words, defects with $N \neq 0$ are stable.

3) $N = 0$: Topologically trivial. As I promised at the beginning that topological classification is not limited to particular object or system. They apply to any object which meet to requisite symmetry criteria.

For example, topological classification of any object in terms of vorticity is only possible when the associated vector field is confined in a plane.

Examples:

i) whirlpools in lake or ocean, eye of hurricanes : Vortex defects at macroscale.

ii) Spin texture in an xy magnet the phase of the spin $\theta(\vec{r})$ can wind to produce vortex and/or anti-vortex. The U(1) phase of a superfluid:

Kosterlitz - Thouless transition.

It is important to discuss the KT transition, even if briefly, to appreciate the role topology in condensed matter physics. We assume that the amplitude of superfluid order is fixed Φ_0. It's U(1) phase variable

$$\theta = N\phi = N\tan^{-1}(y/x) \Rightarrow \vec{\nabla}\theta = N\vec{F} = \frac{N}{r}\hat{\phi}$$

Therefore, the energy of a single vortex in a system of linear size R in the continuum approximation is

$$H_v = \frac{\Phi_0^2}{2}\int d^2\vec{r}\,(\vec{\nabla}\theta).(\vec{\nabla}\theta) = \frac{\Phi_0^2 N^2}{2}\cdot 2\pi\int_{r_0}^{R}\frac{r\,dr}{r^2}$$

$$\Rightarrow H_v = \pi\Phi_0^2 N^2 \ln(R/r_0).$$

Here, r_0 is a short distance cut-off which is

proportional to the lattice spacing (a). But for continuum approximation to be sensible $r_0 >> a$.

Therefore, H_V excludes the finite part of the vortex energy arising from the vicinity of the core of vortex, called the core energy. So, in the thermodynamic limit $R \to \infty$ the energy of isolated vortex and anti-vortex diverges. Thus, it is natural to anticipate that at low temperature vortices are indeed negligible in a large system.

However, the presence of vortices increases the entropy of the system. The Boltzmann entropy of a single vortex is

$$\Delta S_V = k_B \ln (R/r_0)^2$$

as the center of the vortex can be placed at the center of $(R/r_0)^2$ plaquett. Therefore, increase of the free-energy due to an isolated vortex is

$$\Delta F_V = H_V - T\,\Delta S_V = \pi \Phi_0^2 N^2 \ln\left(\frac{R}{r_0}\right) - 2 k_B T \ln \frac{R}{r_0}$$

Notice that both the energy and entropy depend "logarithmically" on the system size. Therefore, the free energy changes sign at temperature

$$T_{KT} = \frac{\pi \Phi_0^2 N^2}{2 k_B}$$: Kosterlitz-Thouless transition temperature.

Note that the free energy and T_{KT} is minimum for vortex or anti-vortex of unit vorticity ($N=1$). So, from now on we assume $N=1$. So, for $T > T_{KT}$ vortices become favorable due to the entropy term and free vortices appear in the system. For $T < T_{KT}$

isolated vortices or anti-vortices become unimportan-t due to prohibitively large energy. Assuming that there is a single phase transition at $T = T_{KT}$ between high temperature disordered phase and low temperature (algebraic) phase, we can identify this transition associated with the appearance of free vortices in the system.

However, in reality for $T < T_{KT}$ pairs of vortex-antivortex appear, such that the net vorticity far away from such pairs is Zero. Such configuration costs finite energy and becomes energetically favored at low $T < T_{KT}$. As T_{KT} is approached from below thermal fluctuation gives birth to numerous vortex-antivortex pairs & eventually they become free for $T > T_{KT}$.

For further reading consult:

1) J. M. Kosterlitz and D. J. Thouless, Journal of Physics C, 6, 1181 (1973).
2) A Modern approach to Critical Phenomena, Igor F. Herbut (Cambridge university Press).

iii) The lattice grids, we displayed in Fig. 1(a) & Fig. 1(b) can be large scale latitude & longitude when describing vortex, representing eye of hurricanes or real space square lattice when describing XY magnet or superfluid.

Now, we will discuss how such defects can appear in the reciprocal or momentum space, where $x \to k_y$ and $y \to k_y$. In that case, vortex or anti-vortex defect appears at some point in the Brillouin zone. The question is, when do we see such defects in the momentum space? An affirmative answer to this question can be found by considering Dirac or Weyl Hamiltonian in two dimensions:

$$H = \hbar v_F (\vec{k} \times \vec{\sigma}) \cdot \hat{z} = \hbar v_F (-k_y \sigma_x + k_x \sigma_y),$$

where $\hbar = h/2\pi$ is the reduced Planck constant and v_F is the Fermi velocity. The above Hamiltonian can also be written as $H = \hbar v_F \vec{d}(k) \cdot \vec{\sigma}$, where $\vec{d}(k) = (-k_y, k_x) = k(-\sin\phi_k, \cos\phi_k)$ with ϕ_k as the polar or azimuthal angle in the momentum space and $\vec{\sigma} = (\sigma_1, \sigma_2)$ is the vector Pauli matrix.

First, we compute the eigenvalues of H. For that we square the Hamiltonian:

$$H^2 = \hbar^2 v_F^2 \left(k_y^2 \sigma_x^2 + k_x \sigma_y^2 - k_x k_y (\sigma_x \sigma_y + \sigma_y \sigma_x) \right).$$

Recall that Pauli matrices satisfy the algebra

$$\{\sigma_j, \sigma_k\} = 2\delta_{jk} \quad \& \quad [\sigma_j, \sigma_k] = i\epsilon_{jkl}\sigma_l$$

where ϵ_{jkl} is the anti-symmetric Levi-Cevita tensor $\Rightarrow \sigma_x^2 = \mathbb{1} = \sigma_y^2$ & $\sigma_x \sigma_y + \sigma_y \sigma_x = 0$

Since, the eigenvalues of H are energies $\{E\}$, so eigenvalues of H^2 are $\{E^2\}$. Therefore,

$$E^2 = \hbar^2 v_F^2 (k_x^2 + k_y^2) \Rightarrow E = \pm \hbar v_F \sqrt{k_x^2 + k_y^2}$$
$$= \pm \hbar v_F |k| .$$

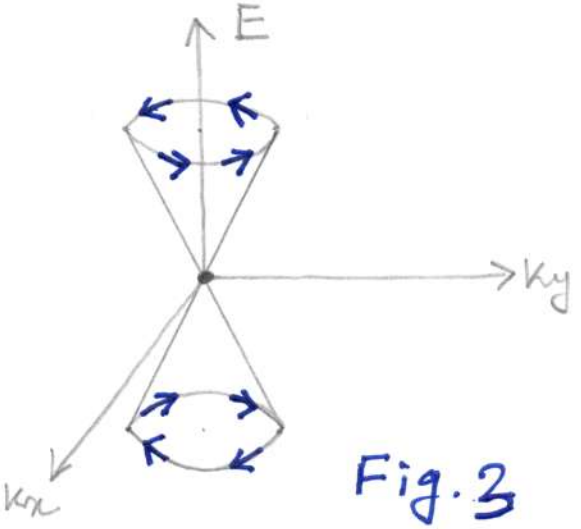

Fig. 3

The energy spectra E as a function of momenta $\vec{k} = (k_x, k_y)$ are shown in Fig. 3. Note that there is a positive energy branch: hole or conduction band & there is a negative energy branch: electron or valence band.

Before, we delve into revealing the topology of Dirac or Weyl band, let us summarize a few important observations from the computation of energy eigenvalues of H:

a) Consider a generic Hamiltonian in any dimension

$$H = d_1(\vec{k})\,\Gamma_1 + d_2(\vec{k})\,\Gamma_2 + \dots$$

where, $d_j(\vec{k})$ are assumed to be arbitrary regular function of momentum $\vec{k}$ and Γ matrices satisfy the anti-commuting Clifford algebra:

$$\{\Gamma_j, \Gamma_k\} = 2\,\delta_{jk}$$

b) Then eigenvalues of H, given by $\{E\}$ can be obtained by squaring the Hamiltonian, given by

$$H^2 = E^2 = d_1^2 \Gamma_1^2 + d_2^2 \Gamma_2^2 + d_1 d_2 (\Gamma_1\Gamma_2 + \Gamma_2\Gamma_1) + \dots$$

Here, for brevity we set $d_j(\vec{k}) \equiv d_j$

By the virtue of anti-commuting algebra all the cross terms vanish pairwise & $\Gamma_1^2 = \Gamma_2^2 = \ldots = \mathbb{1}$.

Therefore, $E^2 = d_1^2 + d_2^2 + \ldots \Rightarrow \boxed{E = \pm\sqrt{d_1^2 + d_2^2 + \ldots}}$

c) We can extract the degeneracy of the valence band (with $E<0$) and the conduction band (with $E>0$) in the following way:

If the dimensionality of the Γ matrices is 2^n, where n is positive integer, then conduction band is 2^{n-1} fold degenerate & valence band is 2^{n-1} fold degenerate. $\Rightarrow$ Total $2 \times 2^{n-1} = 2^n$ eigenvalues.

(valence & conduction band; degeneracy)

In case of the Dirac or Weyl Hamiltonian we discussed previously $n = 1$. So, the valence and conduction bands are 1-fold degenerate or non-degenerate.

d) Another important theorem worth mentioning. If the dimensionality of mutually anti-commuting Hermitian Γ matrices, satisfying the Clifford algebra $\{\Gamma_j, \Gamma_k\} = 2\delta_{jk}$, is 2^n where n is a positive integer then there exists $(2n+1)$ number of such mutually anti-commuting matrices. Out of them $(n+1)$ can be chosen to be purely real & n to be purely imaginary. Consider, Pauli matrices $\Rightarrow n = 1$. There are 3 mutually anti-commuting Pauli matrices $(\sigma_x, \sigma_y, \sigma_z)$. Two are purely real: σ_x & σ_z. One is purely imaginary: σ_y.

Now, we return to the discussion on the two-component Dirac & Weyl Hamiltonian: The normalized eigenvectors for the conduction & valence bands are respectively

$$|+E\rangle = \frac{1}{\sqrt{2}} \begin{pmatrix} \hat{d}_1 - i\hat{d}_2 \\ 1 \end{pmatrix} \quad \text{and} \quad |-E\rangle = \frac{1}{\sqrt{2}} \begin{pmatrix} \hat{d}_1 + i\hat{d}_2 \\ 1 \end{pmatrix},$$

where $\hat{d} = \vec{d}/|\vec{d}| = (\hat{d}_1, \hat{d}_2)$. The projection operators to the conduction (+) and valence (-) bands are respectively

$$P_{\pm} = |\pm E\rangle\langle \pm E| = \frac{1}{2}\left(\mathbb{1} \pm \hat{d}\cdot\vec{\sigma}\right).$$

Finally, we compute the expectation value of the spin operator $\vec{S} = \vec{\sigma}/2$ in the conduction & valence bands, respectively given by

$$\langle \vec{S} \rangle_{\pm} = Tr\left[\vec{S}\, P_{\pm}\right] = \pm \frac{\hat{d}}{2} = \pm \left(-\sin\phi_k, \cos\phi_k\right)$$
$$\equiv \pm \vec{F}$$

Thus, to topologically characterize the conduction & valence band we compute

$$\frac{1}{2\pi} \oint_C \langle \vec{S} \rangle_{\pm} \cdot d\vec{l} = \pm 1,$$

where now the closed line integral is taken over a closed contour in the momentum space & the square lattice $\Rightarrow$ discretized version of the Brillouin zone..

This phenomenon is called Spin-momentum locking And Dirac or Weyl point is the core of such vortex, a singular point in the Brillouin zone.

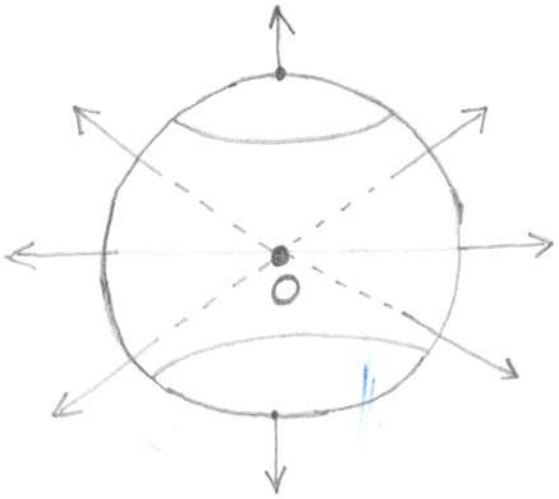

Fig. 4

Next, we consider a three-dimensional defect characterized by the vector field

$$\vec{F} = \frac{1}{r^3}(x, y, z)$$

$$= \frac{1}{r^2}(\sin\theta\cos\phi, \sin\theta\sin\phi, \cos\theta)$$

where $r^2 = x^2 + y^2 + z^2$. In spherical polar co-ordinates:

$$\vec{F} = \frac{1}{r^2}\hat{r}$$

A schematic representation of such vector field is shown in Fig. 4. Field lines come out from the origin O that are distributed over the surface of sphere uniformly. Next we compute the closed surface integral of $\vec{F}$ over the surface of a sphere of radius R (arbitrary):

$$\oint_S \vec{F}.d\vec{a} = \int_{\phi=0}^{2\pi}\int_{\theta=0}^{\pi} \frac{1}{R^2} R^2 \sin\theta\, d\theta\, d\phi = 4\pi.$$

Now, lets compute the same integral using the divergence theorem. But, notice that

$$\vec{\nabla}.\vec{F} = \frac{1}{r^2}\frac{\partial}{\partial r}\left(r^2\frac{1}{r^2}\right) = \frac{1}{r^2}\frac{\partial}{\partial r}(1) = 0.$$

$$\Rightarrow \int_V (\vec{\nabla}.\vec{F})\, dV = 0 !$$

Paradoxical result (?) NO

Note that $\vec{\nabla}.\vec{F} = 0$ everywhere in the space but at the origin $r = 0$. Therefore, origin represents a "core" of another type of topological defect, named "hedgehog" and its core is named monopole. For an anti-hedgehog, its core is called anti-monopole & the vector field associated with it is given by $\vec{F} = -\frac{1}{r^2}\hat{r}$.

The quantity we computed in terms of the surface integral, determines the topological invariant of hedgehog or anti-hedgehog, given by.

$$N = \frac{1}{4\pi} \oint_S \vec{F}.\,d\vec{a} = \pm 1$$

For anti-hedgehog, the field lines point toward the origin (contrast with Fig. 4).

Now, the question is where in nature we can find hedgehog topological defect? First answer is in animal kingdom! Second example can be found, if we now consider three-dimensional Dirac or Weyl Hamiltonian:

$$H = (\vec{\sigma}.\vec{k})\,\hbar v_F = \hbar v_F (\sigma_1 k_x + \sigma_2 k_y + \sigma_3 k_3)$$
$$\equiv \hbar v_F\, \vec{\sigma}.\,\vec{d}(k).$$

Energy spectra: $E = \pm \hbar v_F \sqrt{k_x^2 + k_y^2 + k_z^2}$

$$= \pm \hbar v_F |\vec{k}|$$

The Hamiltonian can also be written as.

$H = \hbar v_F k \, (\hat{d}(k) \cdot \vec{\sigma})$, where $\hat{d}(\vec{k}) = (\sin\theta_k \cos\phi_k, \sin\theta_k \sin\phi_k, \cos\theta_k)$

where θ_k and ϕ_k are the polar and azimuthal angles in the reciprocal space or momentum space. The normalized wavefunctions for the conduction & valence bands are respectively

$$|+E\rangle = \frac{1}{\sqrt{2}} \begin{pmatrix} \dfrac{\hat{d}_1 - i\hat{d}_2}{\sqrt{1-\hat{d}_3}} \\ \sqrt{1-\hat{d}_3} \end{pmatrix} \quad \text{and} \quad |-E\rangle = \frac{1}{\sqrt{2}} \begin{pmatrix} -\dfrac{\hat{d}_1 - i\hat{d}_2}{\sqrt{1+\hat{d}_3}} \\ \sqrt{1+\hat{d}_3} \end{pmatrix}$$

Therefore, the projection operators on the conduction and valence bands are respectively

$$P_{\pm} = |\pm E\rangle\langle \pm E| = \frac{1}{2} \left(\mathbb{1} \pm \hat{d} \cdot \vec{\sigma} \right)$$

Therefore, the expectation value of the spin-operators in the conduction & valence bands are respectively

$$\langle \vec{S} \rangle_{\pm} = Tr\left[\vec{S} \, P_{\pm} \right] = \pm \frac{\hat{d}}{2} \equiv \pm (\sin\theta_k \cos\phi_k, \sin\theta_k \sin\phi_k, \cos\theta_k)$$

Topological characterization of the conduction and valence bands is provided by the invariant

$$\frac{1}{4\pi} \oint_S \langle \vec{S} \rangle_{\pm} \cdot \vec{da} = \pm 1 .$$

Therefore, along a constant energy contour, which is a sphere now, the spin projection along various directions combine to take the [redacted] shape of a (anti-)hedgehog and three dimensional Weyl point acts as a monopole in a 3D momentum space.

Lets now take a brief pause and [redacted] summarize what we have learn in the last two examples:

1) As seen from the conduction band, the Weyl point in two dimensions acts as the core of a vortex in the momentum space.
2) As seen from the conduction band, the Weyl point in three dimensions. acts as the core of a hedgehog, also known as monopole in the momentum space.

Although, [redacted] when seen from the valence band vortex → anti-vortex & hedgehog → anti-hedgehog, but for topological characterization of point defect, we need to fix the band. In real space it is equivalent to looking at the defect either from the top or the bottom.

Therefore, we found either vortex like defect in 2D or hedgehog like defect in 3D. But, during the discussion on KT transition, we heard about vortex-anti-vortex bound state.

So, when do we see anti-vortex or anti-hedge-hog in momentum space? It turns out that lattice models for Dirac & Weyl fermions always produce a pair of vortex-anti-vortex (in 2D) or hedgehog-anti-hedgehog (in 3D) : Nielsen-Ninomiya no-go theorem, but there are exceptions, which we will discuss later.

Let us first consider a concrete lattice model to exemplify the Nielsen-Ninomiya no-go theorem : Graphene's honeycomb lattice. The crystal structure and the Brillouin zone are shown below

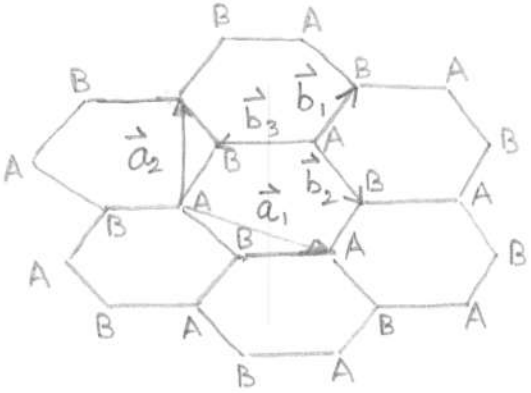

Fig. 5(a)

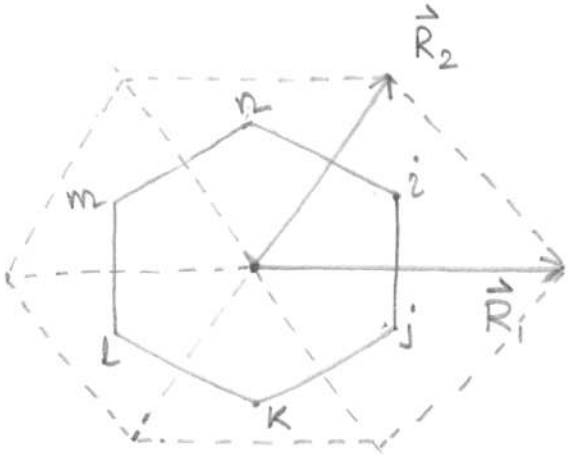

Fig. 5(b)

The first object we need to appreciate about lattice structure or crystallography is Bravais lattice : Infinite array of discrete points generated by a set of discrete translation operations, described by $\vec{T} = n_1 \vec{a}_1 + n_2 \vec{a}_2$, where n_i are integers & $\vec{a}_i$ are (primitive) translation vectors.

Honeycomb lattice is not a Bravais lattice (BT). The underlying BT is the triangular lattice & honeycomb lattice ≡ Interpenetrating triangular lattices, denoted by A and B, as shown in Fig. 5(a).

The premitive translational vectors are:

$$\vec{a}_1 = \left(\frac{\sqrt{3}}{2}, -\frac{1}{2}\right) a \quad \text{and} \quad \vec{a}_2 = (0, 1)\, a.$$

where a is the lattice spacing. Two triangular lattices are called sublattices. The nearest-neighbor (NN) sites belong to A and B sublattices, and they are connected by the vectors:

$$\vec{b}_1 = \left(\frac{1}{2\sqrt{3}}, \frac{1}{2}\right) a, \quad \vec{b}_2 = \left(\frac{1}{2\sqrt{3}}, -\frac{1}{2}\right) a$$

$$\text{and} \quad \vec{b}_3 = \left(-\frac{1}{\sqrt{3}}, 0\right) a.$$

These three NN vectors are also shown in Fig. 5(a). Note that the B sites are generated from A sites by $\vec{B}(n_1, n_2) = n_1 \vec{a}_1 + n_2 \vec{a}_2 + \vec{b}_1$. Due to the translational symmetry of lattice or crystals, we often go to momentum space, known as Brillouin zone (BZ). The BZ for the [redacted] triangular lattice is honeycomb lattice in momentum space. Thus, for honeycomb lattice, we get two superimpose copies of the same BZ, shown in Fig. 5(b). The reciprocal lattice vectors are

$$\vec{R}_1 = \frac{4\pi}{\sqrt{3}a}(1, 0) \quad \text{and} \quad \vec{R}_2 = \frac{4\pi}{\sqrt{3}a}\left(\frac{1}{2}, \frac{\sqrt{3}}{2}\right)$$

Identified sides of the BZ are : $ij \equiv lm$, $jk \equiv mn$ and $kl \equiv ni$. And two sets of inequivalent corners of the BZ are $i \equiv k \equiv m$ & $j \equiv l \equiv n$. See Fig. 5(b) for reference.

Upon establishing the crystallo-graphic description of honeycomb lattice, we proceed to capture the its electronic properties in terms of the simplest model in solid state physics, the tight-binding model with only nearest-neighbor hopping processes with amplitude t_0 :

$$H_{TB} = t_0 \sum_{\vec{A}, i} c^{+}_{\vec{A}} c_{\vec{A}+\vec{b}_i} + H.c.$$

where $c^{+}_{\vec{A}}$ is the fermion creation operator on the sites of A sublattice and $c_{\vec{A}+\vec{b}_i}$ is the fermionic annihilation operator on its three neighboring sites belonging to the B sublattice. Note that graphene is a monatomic lattice with all the sites being occupied by carbon atoms. Hence, there is no difference between the on-site energies for the A and B sites. Still, to facilitate a forthcoming discussion, I add a staggered potential term

$$H_{SP} = \beta \sum_{\vec{A}} \left(c^{+}_{\vec{A}} c_{\vec{A}} - c^{+}_{\vec{A}+\vec{b}_1} c_{\vec{A}+\vec{b}_1} \right)$$

β is the difference between the onsite energies for the A and B sites.

For the moment, we ignore the spin degrees of freedom. Using the Fourier transform, we write

$$c_{\vec{A}} = \int_{BZ} \frac{d^2\vec{k}}{(2\pi)^2} e^{i\vec{k}.\vec{A}} U(\vec{k}).$$

↳ Annihilation operator on A sites with momentum $\vec{k}$

$$c_{\vec{B}} = \int_{BZ} \frac{d^2\vec{k}}{(2\pi)^2} e^{i\vec{k}.\vec{B}} V(\vec{k})$$

↳ Annilation operator on B sites with momentum $\vec{k}$.

Lets consider the term.

$$t_0 \sum_{\vec{A}, i=1,2,3} c^{\dagger}_{\vec{A}} c_{\vec{A}+\vec{b}_i} = t_0 \sum_{i=1}^{3} \int_{BZ} \frac{d^2\vec{k}}{(2\pi)^2} \int_{BZ} \frac{d^2\vec{q}}{(2\pi)^2} U^{\dagger}(\vec{k}) e^{i\vec{k}.\vec{A}} e^{-i\vec{q}.(\vec{A}+\vec{b}_i)} V(\vec{q}) + H.c.$$

$$= t_0 \sum_{i=1}^{3} \int_{BZ} \frac{d^2\vec{k}}{(2\pi)^2} \int \frac{d^2\vec{q}}{(2\pi)^2} e^{i(\vec{k}-\vec{q}).\vec{A}} U^{\dagger}(\vec{k}) e^{-i\vec{q}.\vec{b}_i} V(\vec{q}) + H.c.$$

$$= t_0 \int_{BZ} \frac{d^2\vec{k}}{(2\pi)^2} U^{\dagger}(\vec{k}) \left(e^{-i\vec{k}.\vec{b}_1} + e^{-i\vec{k}.\vec{b}_2} + e^{-i\vec{k}.\vec{b}_3} \right) V(\vec{k}) + H.c.$$

Following this procedure, we can write the total Hamiltonian $H_0 = H_{TB} + H_{SP}$ as.

$$H_0 = \int_{BZ} \frac{d^2\vec{k}}{(2\pi)^2} \begin{pmatrix} U^{\dagger}(\vec{k}) & V^{\dagger}(\vec{k}) \end{pmatrix} \begin{pmatrix} \beta & t_0 \sum_{i=1}^{3} e^{-i\vec{k}.\vec{b}_i} \\ t_0 \sum_{i=1}^{3} e^{+i\vec{k}.\vec{b}_i} & -\beta \end{pmatrix} \begin{pmatrix} U(\vec{k}) \\ V(\vec{k}) \end{pmatrix}$$

$$\equiv h(\vec{k}).$$

where $h(\vec{k}) = \beta\sigma_3 + t_0 \mathrm{Re}[f(k)]\sigma_1 + t_0 \mathrm{Im}[f(k)]\sigma_2$

and $f(k) \equiv \sum_{i=1}^{3} \exp(-i\vec{k}.\vec{b}_i)$.

After some straight forward algebra, it can be shown that

$$\mathrm{Re}[f(k)] = \cos\left(\frac{k_x a}{\sqrt{3}}\right) h_1(k_x, k_y) + 2\sin\left(\frac{k_x a}{\sqrt{3}}\right) h_2(k_x, k_y)$$

$$\mathrm{Im}[f(k)] = 2\cos\left(\frac{k_x a}{\sqrt{3}}\right) h_2(k_x, k_y) - \sin\left(\frac{k_x a}{\sqrt{3}}\right) h_1(k_x, k_y)$$

where, $h_1(k_x, k_y) = 1 + 2\cos\left(\frac{\sqrt{3}\,k_x a}{2}\right)\cos\left(\frac{k_y a}{2}\right)$

& $h_2(k_x, k_y) = \sin\left(\frac{\sqrt{3}\,k_x a}{2}\right)\cos\left(\frac{k_y a}{2}\right)$.

The Bloch Hamiltonian $h(\vec{k})$ is expressed in terms of three mutually anti-commuting Hermitian Pauli matrices $\Rightarrow$ Eigenvalues of $h(\vec{k})$ are $\pm E(\vec{k})$, where $E(\vec{k}) = \left[\beta^2 + \mathrm{Re}[f(k)]^2 + \mathrm{Im}[f(k)]^2\right]^{1/2}$

Now, we set $\beta = 0$. Then $E(\vec{k}) = 0$ at SIX corners of the BZ, which we marked as i, j, k, l, m and n in Fig. 5(b). However, we already learned that not all six corners of the BZ are inequivalent. Specifically, corners i, k and m are related by linear combinations of reciprocal lattice vectors $\vec{R}_1$ and $\vec{R}_2$. Similarly, j, l & n are related by linear combination of $\vec{R}_1$ and $\vec{R}_2$. Thus, we need to take into account only TWO inequivalent corners. We choose them to be i at momentum $\vec{k}_1 = \frac{4\pi}{\sqrt{3}a}\left(\frac{1}{2}, \frac{1}{2\sqrt{3}}\right)$ and l at [redacted] $\vec{K}_2 = -\vec{K}_1$. In order to obtain an effective Hamiltonian around two valleys at $\pm\vec{K}_1$,

We linearize (Taylor expansion) $h(\vec{k})$ around these two points. Around the valleys $\pm\vec{K}_1$, we denote the linearize Hamiltonian by $h_\pm(\delta\vec{k})$, respectively, where

$$h_\pm(\delta\vec{k}) = \mp\left(\frac{\sqrt{3}}{2}t_0 a\right)\left[\left(\frac{\sqrt{3}}{2}\delta k_x + \frac{1}{2}\delta k_y\right)\sigma_1 \pm \left(\frac{\sqrt{3}}{2}\delta k_x + \frac{1}{2}\delta k_y\right)\sigma_2\right] + \beta\sigma_3.$$

where $\delta\vec{k} = \vec{k} \mp \vec{K}_1$. Now, go to a rotated frame of momentum $\vec{q}$, such that

$$\begin{pmatrix} q_x \\ q_y \end{pmatrix} = \begin{pmatrix} \cos\theta & \sin\theta \\ -\sin\theta & \cos\theta \end{pmatrix}\begin{pmatrix} \delta k_x \\ \delta k_y \end{pmatrix}$$

with $\theta = \pi/6$. This rotation is shown in Fig. 5(c). In terms of $\vec{q}$ vector:

$$h_\pm(\vec{q}) = \mp\left(\frac{\sqrt{3}}{2}t_0 a\right)\left(q_x\sigma_1 \pm q_y\sigma_2\right) + \sigma_3\beta.$$

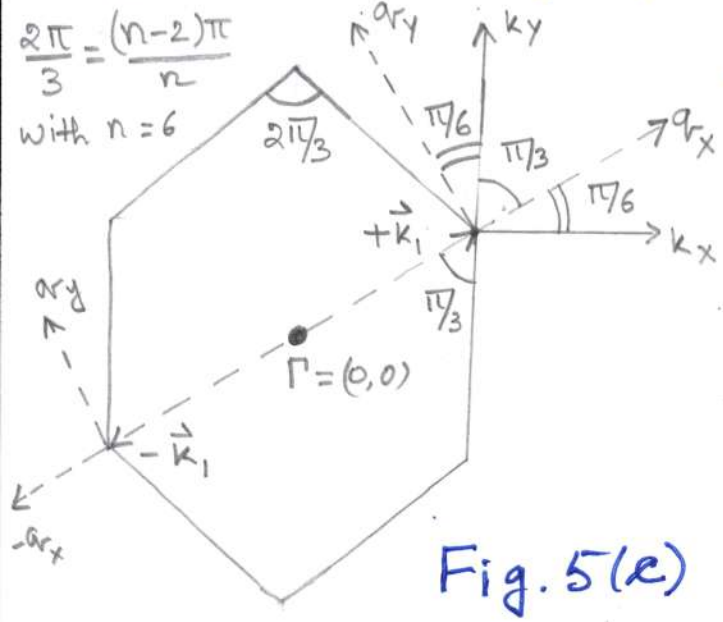

Fig. 5(c)

Note that $|\delta\vec{k}| << |\vec{K}_1|$ and $|\vec{q}| << |\vec{K}_1|$. The quantity $(\sqrt{3}/2\, t_0 a)$ is the Fermi velocity v_F of Weyl Fermions. After resotoring the factor of $\hbar$ we find

$$v_F = \frac{\sqrt{3}}{2}(t_0 a/\hbar) \approx 10^6\ m/s$$

with $t \approx 3\,eV$ and $a \approx 2.46\,\text{Å}$. Thus, we have two-component Weyl fermions near each valley at $+\vec{K}_1$ and $-\vec{K}_1$. But the effective Fermi velocity $v_F << c$ (speed of light). To appreciate the topology of these two Dirac/Weyl points, we now

Unitarily rotate $h_\pm(\vec{q})$ by the Unitary matrix $U = \exp\left(i\frac{\pi}{4}\sigma_3\right)$, yielding

$$\tilde{h}_\pm(\vec{q}) = U\, h_\pm(\vec{q})\, U^\dagger = v_F\left(-q_y\sigma_1 \pm q_x\sigma_2\right) + \beta\sigma_3$$
$$\equiv v_F|\vec{q}|\left(-\sin\phi_k^r\,\sigma_1 \pm \cos\phi_k\,\sigma_2\right) + \beta\sigma_3.$$

Now, you can apply the algebra I showed you before to show that when $\beta = 0$

$$\frac{1}{2\pi}\oint_C \langle\vec{S}\rangle_+ \cdot d\vec{l} = \pm 1 .$$

The '+' sign on the left hand side denotes that we commit to the conduction band, and '$\pm$' sign on the right hand side correspond to the $\pm\vec{K}$, valley, respectively. Therefore, in a lattice model of massless Dirac fermions, there are two Dirac points (always). In 2D, one of them corresponds to a vortex object in the BZ, while the other one corresponds to anti-vortex. So, the net vorticity in the entire 2D BZ is ZERO. Hence, a stable Dirac system in 2D is a bound state of vortex and anti-vortex in the momentum space. This is an example of Nielsen-Ninomiya no-go theorem. Exactly the same outcome holds in 3D, where a stable Weyl system features a monopole & anti-monopole in the momentum space, & it is a bound state of monopole-antimonopole in the momentum space.

Before, leaving the discussion on graphene let's discuss how one can cast the effective Dirac Hamiltonian in relativistic notation:

The total Hamiltonian (linearized) obtained by taking contributions from $\pm \vec{K}_1$ valley reads

$$h_{total}(\vec{q}) = \begin{array}{c|c} h_+(\vec{q}) & \\ \hline & h_-(\vec{q}) \end{array} = \begin{array}{c|c} -v_F(q_x\sigma_1 + q_y\sigma_2) + \beta\sigma_3 & \\ \hline & v_F(q_x\sigma_1 - q_y\sigma_2) + \beta\sigma_3 \end{array}$$

$$\Rightarrow h_{total}(\vec{q}) = +v_F q_x \begin{array}{c|c} -\sigma_1 & \\ \hline & \sigma_1 \end{array} + v_F q_y \begin{array}{c|c} -\sigma_2 & \\ \hline & -\sigma_2 \end{array} + \beta \begin{array}{c|c} \sigma_3 & \\ \hline & \sigma_3 \end{array}.$$

$$\equiv v_F q_x (-\tau_3 \otimes \sigma_1) + v_F q_y (-\tau_0 \otimes \sigma_2) + \beta(\tau_0 \otimes \sigma_3)$$

The 2-component Pauli matrices $\{\tau_\mu\}$ operate on the valley index. Now, we define mutually anti-commuting 4-component Hermitian γ matrices:

$$\gamma_0 = \tau_0 \otimes \sigma_3, \quad \gamma_1 = -\tau_3 \otimes \sigma_2, \quad \gamma_2 = \tau_0 \otimes \sigma_1.$$

To complete the clifford algebra of 5 mutually anti-commuting γ matrices we also define

$$\gamma_3 = \tau_1 \otimes \sigma_2 \quad \text{and} \quad \gamma_5 = \tau_2 \otimes \sigma_2.$$

Together they satisfy $\{\gamma_\mu, \gamma_\nu\} = 2\delta_{\mu\nu}$. And the Hamiltonian reads as

$$H_D = v_F\left(\psi^\dagger_{\vec{q}}\, i\gamma_0\gamma_1 q_x \psi_{\vec{q}} + \psi^\dagger_{\vec{q}}\, i\gamma_0\gamma_2 \psi_{\vec{q}}\right) + \beta\psi^\dagger_{\vec{q}}\gamma_0\psi_{\vec{q}}$$

$$= v_F \sum_{j=1}^{d} \overline{\psi}_{\vec{q}}\, i\gamma_j q_j \psi_{\vec{q}} + \beta\, \overline{\psi}_{\vec{q}}\psi_{\vec{q}}$$

where $\bar{\Psi}_{\vec{q}} = \Psi^{\dagger}_{\vec{q}} \gamma_0$ and the 4-component Dirac spinor is $\Psi^{T}_{\vec{q}} = \left[U^{+}_{\blacktriangle}(\vec{q}), V^{+}_{\blacksquare}(\vec{q}), U^{-}_{\blacksquare}(\vec{q}), V^{-}_{\blacksquare}(\vec{q})\right]$.

The [redacted]script [redacted] $\pm$ correspond to two valleys at $\pm\vec{K}$.

The Dirac Hamiltonian H_D enjoys SU(2) global chiral symmetry generated by $\vec{C} = \{\gamma_3, \gamma_5, i\gamma_3\gamma_5\}$, as any unitary rotation (chiral) by arbitrary amount by the generators of the chiral symmetry commutes with H_D, i.e., $\left[\exp\left[i\,\vec{\theta}_{ch}\cdot\vec{C}\right], H_D\right] = 0$

Lagrangian: $L = \sum_{\mu=0}^{d} \bar{\Psi}_{(\vec{q},\omega)}\, i\,\gamma_\mu\, q_\mu\, \Psi_{(\vec{q},\omega)}$, where ω is the Matsubara frequency (fermionic) and $q_\mu = (\omega, v_F\vec{q})$. As there is only a single velocity parameter v_F it can be scaled, by treating v_F as the speed of light. $\Rightarrow$ Lorentz invariant

Reference: G. W. Semenoff, Phys. Rev. Lett. 53, 2449 (1984).

We are now all equipped to turn our focus to insulators when $\beta \neq 0$. In that case, $\langle\vec{S}\rangle_{+} = \frac{\hat{d}}{2} = (-\sin\phi_k, \cos\phi_k, \beta)\frac{1}{\sqrt{v^2k^2+\beta^2}}$

The geometric texture of $\langle\vec{S}\rangle_{+}$ is shown in the next page. [redacted] Here, we considered a single copy of two-component Dirac system for simplicity.

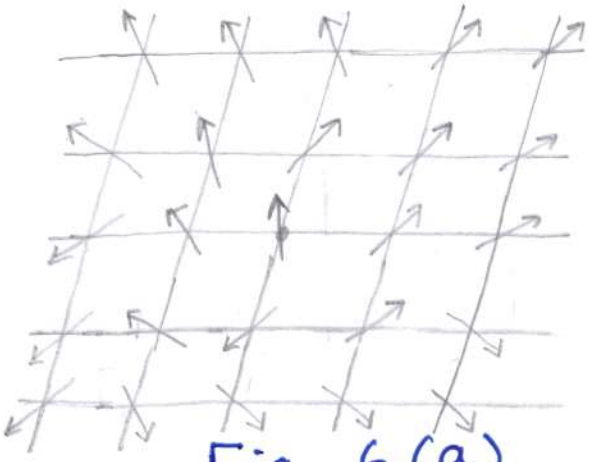

Fig. 6 (a)

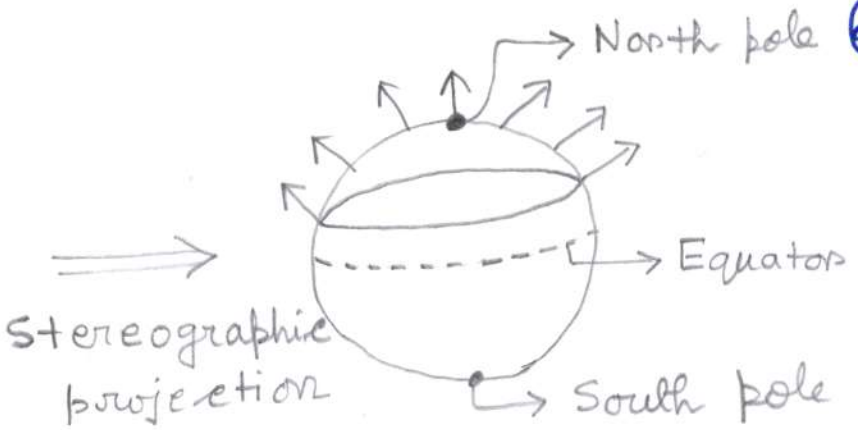

Fig. 6 (b).

Although the planar components of $\langle \vec{S} \rangle_+$ wind around the core of a momentum space lattice, the z-components of $\langle \vec{S} \rangle_+$ sticks them out of plane and in the same direction (say upward) everywhere. As $\langle \vec{S} \rangle_+$ has now 3 components, we can project it on the surface of a sphere, as shown in Fig. 6 (b). Since, ~~none~~ nowhere in the system the z-component of $\langle \vec{S} \rangle_+$ points downward, the $\langle \vec{S} \rangle_+$ vector only partially wraps the sphere. Now, such configeration can be smoothly deformed into one in which all the spins point in one direction, say upward. If we ~~count~~ tag the number of times the spin configuration wraps the whole sphere upon the stereographic projection as the topological invariant ($\mathcal{C}$), then $\mathcal{C} \equiv 0$ in this case. Hence, the Hamiltonian describes a topologically trivial insulator. This conclusion remains unchanged if we add a higher-gradient term taking $\beta \to \beta + bk^2$

with $b > 0$. As it turns out that for topological classification of insulators the higher-gradient terms are very crucial. We can appreciate it even better when considering a mass term $(\beta - bk^2)$ with $b > 0$. Now, the z-component of $\langle \vec{S} \rangle_+$ points in the upward direction at $k = 0$ and in the downward direction at $k \to \infty$, while its planar components wind around the origin. Such texture and its stereographic projection are shown in Fig. 7(a) and 7(b), respectively.

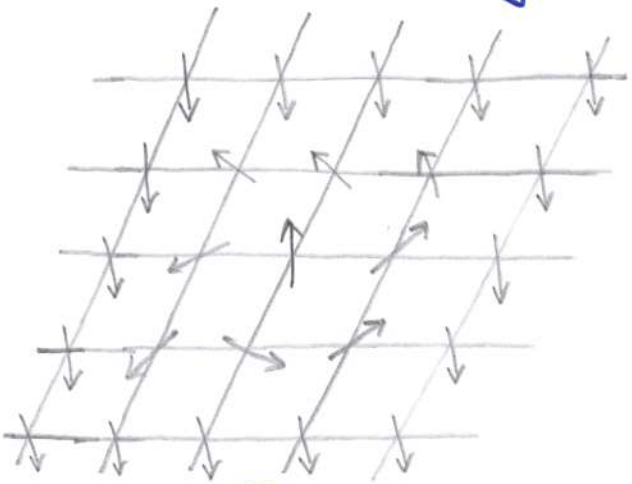

Fig. 7(a)

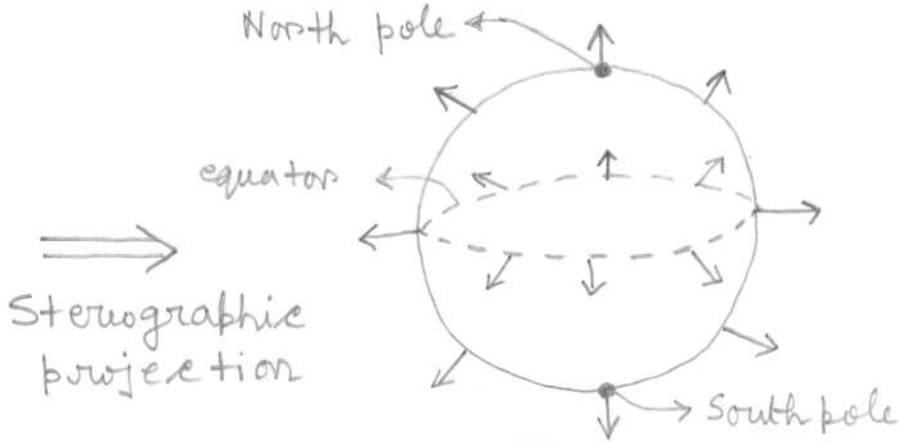

Fig. 7(b)

In this case, the quantity $\langle \vec{S} \rangle_+$ wraps the entire sphere once and thus $C = +1$. Hence, the topological invariant of the underlying insulator is $C = +1$. This is the simplest example of a topological insulator (TI). A $C = -1$ TI can be obtained by flipping the sign of the z-component of $\langle \vec{S} \rangle_+$ everywhere in the system or

by taking $\beta - bk^2 \longrightarrow -(\beta - bk^2)$. As this process involves flipping the direction of an infi-nite number of spins this is not a smooth process. Thus two TIs with $C = +1$ and $C = -1$ are distinct and cannot be smothly deformed in-to each other. Also, both of them are distinct from a trivial insulator with $C = 0$.

The texture of $\langle \vec{S} \rangle_+$ we drew on momentum space lattice or grid is known as Skyrmion. If $C = +1$ configuration is named Skyrmion, then the one with $C = -1$ is called anti-Skyrmion. The skyrmion number in the momentum defines the topological invariant of the insulating state. It's precise mathematical definition is given by

$$C = \frac{1}{4\pi} \int \langle \vec{S} \rangle_+ \cdot \left(\frac{\partial \langle \vec{S} \rangle_+}{\partial k_x} \times \frac{\partial \langle \vec{S} \rangle_+}{\partial k_y} \right) dk_x dk_y$$

$$= \frac{1}{4\pi} \int_{K=0}^{\infty} \int_{\phi_k = 0}^{2\pi} \Omega_{\vec{k}} \; K \, dK \, d\phi \; . = \pm 1, 0.$$

$$\Omega_{\vec{k}} = \frac{v_F^2 (bk^2 + \beta)}{E_k^3}$$

$$E_k = \left[v^2 k^2 + (\beta - bk^2)^2 \right]^{1/2}$$

The vector tripple product inside the integral is called the Berry curvature. Note that for this integral to be ultraviolet convergent $b \neq 0$. It shows the importance of ultraviolet scale physics

in topological classification of solids. The existence of TIs gives rise to another important notion, called the band inversion, which one can appreciate if we track the spin-polarization of the valence or conduction band with momentum. For simplicity, let's focus on the z-component of the spin, as shown in Fig. 8(a) & 8(b):

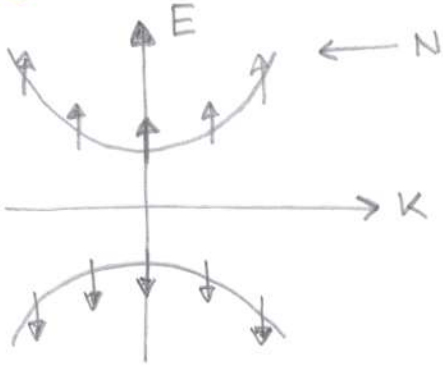

← No band inversion

band inversion at finite momentum

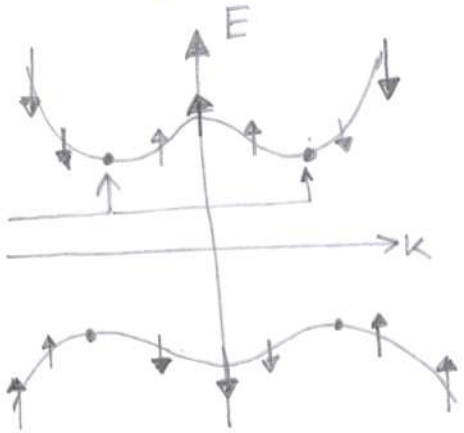

Fig. 8(a)

Fig. 8(b).

In Fig. 8(a), we show the spin polarizations of electronic bands when the mass term is $(\beta + bk^2)$ with $\beta, b > 0$. Clearly the nature of the spin-polarization in the valence or conduction band does not change as a function of momentum (k).

In Fig. 8(b), we show the same quantity, however, for a mass term $(\beta - bk^2)$, with $\beta, b > 0$. Let's focus on the conduction band. For small momentum ($k \to 0$) the spin-polarization is in $+z$ direction in spin space or upward, while at large momentum ($k \to \infty$) it is in the $-z$ direction in the spin space or downward.

At a finite momentum $k_* = \pm\sqrt{\beta/b}$ the nature of the spin-polarization inverts & this phenomenon is called the band inversion. This concept is applicable in any physical dimension. The simplest example we discussed so far is called quantum anomalous Hall insulator (QAHI) or Chern insulator which produces a quantized (in units of e^2/h) Hall conductivity at zero temperature and frequency without any external magnetic field (thus anomalous).

We now show this calculation briefly by displaying the key steps. Some intermediate steps can be found in any regular textbook. To this point, we use the Kubo formula. Recall that the Hamiltonian for QAHI is

$$H(\vec{k}) = v_F(k_x\sigma_x + k_y\sigma_y) + (\beta - bk^2)\sigma_z .$$

The current operator's in the jth direction is obtained via minimal coupling (gauge invariant)

$$J_i = \left.\frac{\partial H(\vec{k} - e\vec{A})}{\partial A_i}\right|_{\vec{A}=0}$$

where e is electronic charge & we set $\hbar = 1$

$$\Rightarrow J_x = -e[v_F\sigma_x - 2bk_x\sigma_z]$$
$$J_y = -e[v_F\sigma_y - 2bk_y\sigma_z]$$

Fermionic Green's function:

$$G(i\omega_n, \vec{k}) = \frac{1}{i\omega_n - H(\vec{k})} = -\frac{i\omega_n + H(\vec{k})}{\omega_n^2 + E^2(\vec{k})}$$

where, $\omega_n = (2n+1)\pi \frac{k_B T}{\hbar}$ with $n = -\infty, \ldots, \infty$ are the fermionic Matsubara frequency, T is the temperature & k_B is the Boltzman constant. We also set $k_B = 1$. In the Kubo formalism to compute the Hall conductivity (σ_{xy}), first we evaluate the transverse polarization bubble

$$\Pi_{xy}(i\omega_\blacksquare) = (-)\, T \sum_{\vec{k}} \int \sum_n \left(J_x\, G(i\omega_\blacksquare + i\nu_n, \vec{k})\, J_y\, G(i\nu_n, \vec{k}) \right)$$

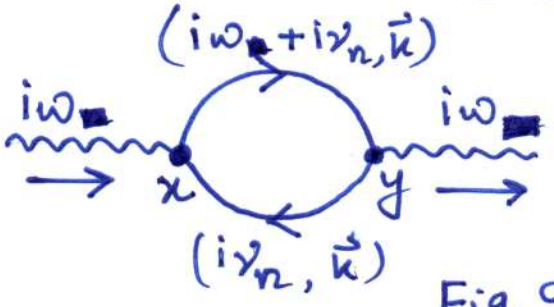

Fig. 9.

The minus (−) sign in front comes due to fermion bubble

Now, we have the choice of computing $\Pi_{xy}(i\omega)$ in two limits: (a) we set $T \to 0$ first & then $\omega \to 0$ which gives dc Hall conductivity in the limit $\omega/T \to \infty$, (b) we set $\omega \to 0$ first & then $T \to 0$, yielding dc Hall conductivity in the limit $\omega/T \to 0$. I show the calculation for $\omega/T \to \infty$. At zero temperature the fermionic Mastubara frequencies form a continuum

$\nu \in (-\infty, \infty)$. & $\sum_{n=-\infty}^{\infty} \longrightarrow \frac{1}{2\pi} \int_{-\infty}^{\infty} d\nu$. Most of the calculation can be now performed straightforwardly using Mathematica. We perform the 'Tr' algebra, integral over ν is computed using the residue theorem, yielding

$$\Pi_{xy}(i\omega) = \blacksquare(-\omega) e^2 \int \frac{d^2\vec{k}}{(2\pi)^2} \frac{2v^2(bk^2+\beta)}{E(k)\left(4E^2(k) - (i\omega)^2\right)}$$

where $E(k) = \sqrt{v_F^2 k^2 + (\beta - bk^2)^2}$. Next step involves the analytic continuation from (imaginary) Matsubara frequency to real frequency $i\omega \longrightarrow \omega + i\eta$ where η is a small real parameter. Then the Hall conductivity within the Kubo formalism reads as

$$\sigma_{xy}(\omega) = \left. \frac{\text{Im}\ \Pi_{xy}(i\omega \to \omega + i\eta)}{\omega} \right|_{\eta \to 0}$$

Here, I now show you how to restore the factors of $\hbar$ or h. In two dimensions conductivity scales in units of e^2/h : guaranteed by gauge invariance. But, we set $\hbar = h/2\pi = 1$. So, ■ in the final step we take $e^2 \longrightarrow e^2/\hbar = (2\pi)(e^2/h)$. The above momentum integral is ultraviolet convergent, which can be computed in Mathematica

giving $\sigma_{xy}(0) = \begin{cases} e^2/h & \text{when } b > 0 \\ 0 & \text{when } b < 0 \end{cases}$ de Hall conductivity.

The coefficient of (e^2/h) is the topological invariant of the underlying insulating state. It can be seen by noting that

$$\sigma_{xy}(0) = \frac{e^2}{h} \cdot \frac{(2\pi) \cdot 2}{(2\pi)^2 \cdot 4} \int \frac{v_F^2 (bk^2 + \beta)}{E_k^3} k\, dk\, d\phi$$

(restoration of $\hbar$; Trace of Pauli matrix; obtained by setting $\omega = 0$; from the measure.)

$$= \left(\frac{e^2}{h}\right) \left(\frac{1}{4\pi}\right) \int \Omega_{\vec{k}}\, k\, dk\, d\phi$$

($\Omega_{\vec{k}}$: Berry curvature.)

C : Momentum space skyrmion number or topological invariant

$$\Rightarrow \boxed{\sigma_{xy}(0) = \frac{e^2}{h} \cdot C \; : \text{ de Hall conductivity}}$$

Let us summarize the outcome in a slightly more convenient notation by assuming $b > 0$ always. Then the phase diagram of $H(\vec{k})$ is the following:

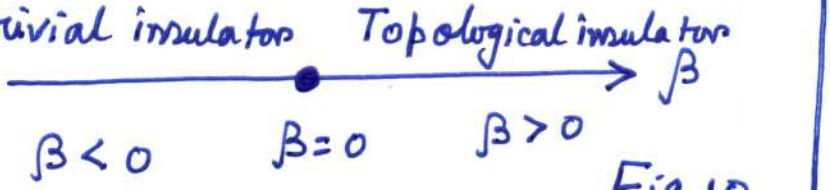

Fig. 10

The quantum phase transition between the topological and trivial insulators take place $\beta = 0$

At this topological quantum critical point (TQCP) the universal Hamiltonian is described by a 2-component massless Dirac fermions:

$$H_{TQCP}(\vec{k}) = v_F(\sigma_x k_x + \sigma_y k_y)$$

It must however be noted that 2-component massless Dirac fermions is NOT a stable phase of matter and they can only be realized as unstable quantum critical excitations at the unstable topological quantum critical point.

Let us cast this scenario in the language of renormalization group (RG). A Dirac theory has dynamic scaling exponent $z = 1$ that determines the relative scaling between energy and momentum according to $E(\vec{k}) = |\vec{k}|^z$. Then all the parameters in the Hamiltonian becomes scale dependent, which we capture by a quantity $l = \ln(\Lambda_0/\Lambda)$, where Λ_0 is a fixed ultraviolet momentum kept fixed and Λ is the running momentum scale at which we measure various parameters. Generically, $v_F = v_F(l)$, $\beta = \beta(l)$ and $b = b(l)$. As one approaches lower momentum or energy l increases monotonically.

The scale dependences of these physical quantities are captured by the RG flow equations

$$\frac{dv_F}{dl} = (z-1)v_F = 0 \quad : \text{marginal when } z=1 \text{ or scale independent}$$

$$\frac{d\beta}{dl} = z\beta \quad : \text{relevant} \Rightarrow \text{gap appears bigger at lower energy scale}$$

$$\frac{db}{dl} = -(z-2)b = -b \Rightarrow \text{irrelevant at lower momentum, where linear in } k\text{-term dominates.}$$

The infrared cut-off (l_*) for the RG flow or maximum value of l is determined by the energy scale up to which fermions exists. In an insulator this scale is determined by the "bare" value of the mass gap $\beta(0)$. Solving the second equation, we find $\beta(l) = \beta(0)\exp(zl)$. and when $\beta(l) = 1$ determines l_* $\Rightarrow l_* = \frac{1}{z}\ln\left(\frac{1}{\beta(0)}\right)$.

Therefore, even ~~though~~ through b is an irrelevant parameter inside an insulator $b(l_*)$ is finite as l_* is finite and renormalized value of $b(l_*)$ always determines the topology. Since, b is a monotonically decreasing function of l as $b(l) = b(0)\exp(-l)$, $b(l) > 0$ when $b(0) > 0$ and vice-versa.

Thus topology of the insulating phase does not alter under RG or it does not depend on the scale of measurement.

On the other hand, at the TQCP $\beta(0) = 0 \Rightarrow l_* \to \infty \Rightarrow b(l \to \infty) = 0$.

For this reason, we neglected the bk^2 term in the universal Hamiltonian for the TQCP in terms of two-component massless Dirac fermions.

If we were to compute the Hall conductivity at the topological QCP, following the Kubo formalism then we should keep the bk^2 term that provides ultraviolet regularization to the momentum integral. Note that for the Hall conductivity the entire filled band contributes and we obtain $\sigma_{xy}^{TQCP}(0) = \frac{1}{2}\frac{e^2}{h}$. Therefore, in terms of the dc Hall conductivity the phase diagram is shown in Fig. 11.

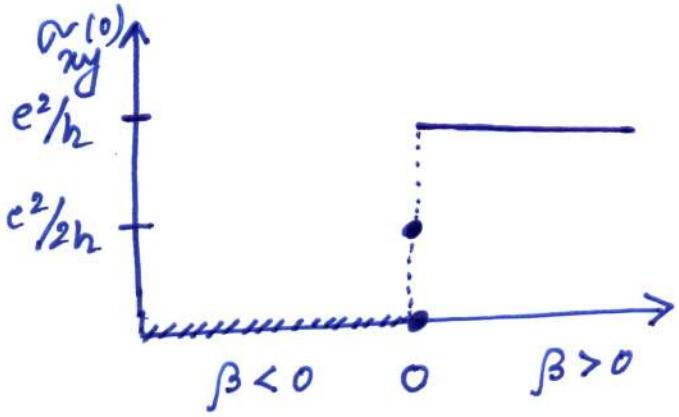

Fig. 11

The TQCP also features a universal longitudinal conductivity, which can be computed at $T=0$ using the Kubo formalism. First we compute

$$\delta\Pi_{xx}(i\omega) = \Pi_{xx}(i\omega) - \Pi_{xx}(0)$$

Here, we subtract the zero external frequency part such that the polarization bubble is free of any ultraviolet divergence. Then,

$$\sigma_{xx}^{TSCP}(\omega) = [\quad] \cdot \frac{\mathrm{Im}\; S\Pi_{xx}(i\omega \to \omega + i\eta)}{\omega} = \frac{e^2}{h} \cdot \frac{\pi}{8}$$

But $\sigma_{xx}(0) = 0$ if $\beta \neq 0$ since the system is an insulator. The question is how come the dc Hall conductivity is quantized despite the bulk of a topological insulator is gapped? The answer to this question rests on the existence of one-dimensional topological edge modes that lives on the boundary of a topological insulator: Bulk-boundary correspondence. This scenario is shown in Fig. 12 & the Hall conductivity is given by $\sigma_{xy} = \frac{I}{V}$. But, in experiments Hall resistivity $R_{xy} = V/I$ is measured.

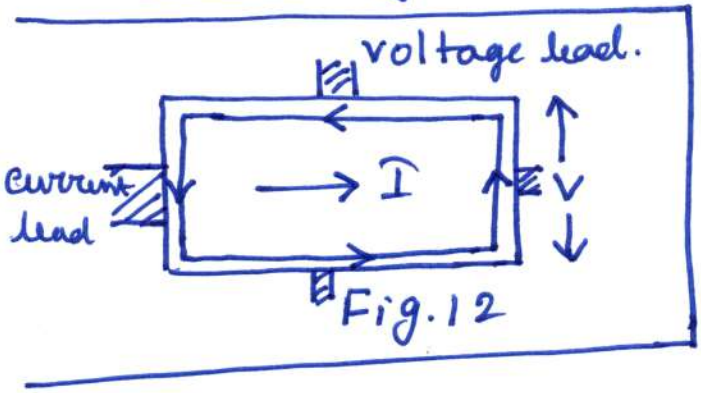

Fig. 12

Next we establish the existence of one-dimensional topological chiral edge mode at the boundaries of a QAHI.

For this purpose, we consider a semi-infinite system with [ ] k_y as a good quantum number. The boundary of the system in the x direction is placed at $x = 0$ (left end) and the region $x > 0$ is occupied

by BAHI. Since the translational symmetry is broken in the x direction $k_x \to -i\partial_x$.

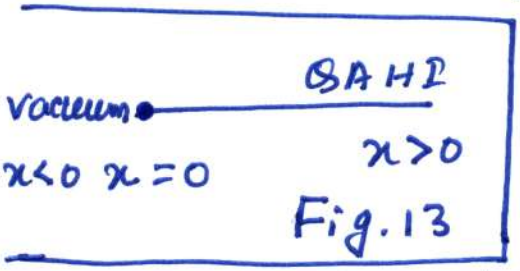

Fig. 13

In the mass term $\beta - b(k_x^2 + k_y^2)$ we set $k_y = 0$ as the band inversion takes place at $k_x = k_y = 0$.

The Hamiltonian operator then reads as.

$$H = v_F(-i\partial_x \sigma_x) + v_F k_y \sigma_y + (\beta + b\partial_x^2)\sigma_z.$$

$$\equiv H(\partial_x) + H(k_y),$$

where $H(\partial_x) = v_F(-i\sigma_x \partial_x) + (\beta + b\partial_x^2)\sigma_z$

and $H(k_y) = (v_F k_y)\sigma_y$.

First, we seek to find the zero-energy mode of the Hamiltonian $H(\partial_x)$ by solving

Superscript 'L' ≡ Left edge

$$H(\partial_x)|\psi_0^L\rangle = 0, \text{ where } |\psi_0^L\rangle = \begin{pmatrix} u^L \\ v^L \end{pmatrix}.$$

But before solving this differential equation let us focus on a few general properties of the zero mode solutions. Say, H is a general Hamiltonian which satisfies a particle-hole symmetry with respect to a unitary or anti-unitary operator P such that $\{P, H\} = 0$. If $|\psi_E\rangle$ is an eigenstate of H with energy E, then $P|\psi_E\rangle \equiv |\psi_{-E}\rangle$ is an eigenstate of H with energy $-E$.

Proof: $H|\Psi_E\rangle = E|\Psi_E\rangle$

$\Rightarrow \underbrace{PH}_{-HP}|\Psi_E\rangle = E(P|\Psi_E\rangle) \Rightarrow H(P|\Psi_E\rangle) = -E(P|\Psi_E\rangle)$.

Now, if the spectrum H supports zero energy mode ($E=0$) then $H|\Psi_0\rangle = 0$ & $H(P|\Psi_0\rangle) = 0$

$\Rightarrow P|\Psi_0\rangle = \pm|\Psi_0\rangle$: $|\Psi_0\rangle$ is an eigenstate of P with eigenvalue $+1$ or -1.

Now, we return to the equation, we had to solve $H(\partial_x)|\Psi_0^R\rangle = 0$. Note that $P = \sigma_y$ as $\{\sigma_y, H(\partial_x)\} = 0$.

$$\Rightarrow \begin{pmatrix} 0 & -i \\ i & 0 \end{pmatrix} \begin{pmatrix} u^R \\ v^R \end{pmatrix} = \pm \begin{pmatrix} u^L \\ v^L \end{pmatrix} \Rightarrow$$

$-iv^R = u^L$ or $iu^L = v^L$: For +

$iv^L = u^L$ or $-iu^L = v^L$: For −

Let's first work with the condition for the '+' sign

$\Rightarrow v_F(-i\partial_x)v^L + (\beta + b\partial_x^2)u^L = 0 \Rightarrow v_F \partial_x u^L + (\beta + b\partial_x^2)u^L = 0$

$v_F(-i\partial_x)u^L - (\beta + b\partial_x^2)v^L = 0 \Rightarrow v_F(-i\partial_x)u^L - i(\beta + b\partial_x^2)u^L = 0$

Therefore, the particle-hole symmetry leads to a single differential equation to be solved

$$v_F \partial_x u^L + (\beta + b\partial_x^2)u^L = 0.$$

Ansatz for localized zero mode: $u \sim e^{-\lambda x}$

$$\Rightarrow \quad b\lambda^2 - v_F\lambda + \beta = 0$$

$$\Rightarrow \quad \lambda = \frac{v_F \pm \sqrt{v_F^2 - 4b\beta}}{2b} \equiv \lambda_\pm^L .$$

General solution: $u(x) = a e^{-\lambda_+ x} + b e^{-\lambda_- x}$

Boundary conditions: (a) $u(x=0) = 0 \Rightarrow b = -a.$

$$\Rightarrow u^L(x) = a\left(e^{-\lambda_+^L x} - e^{-\lambda_-^L x}\right)$$

(b) $u^L(x \to \infty) = 0 \quad \Rightarrow \quad \mathrm{Re}(\lambda_\pm^L) > 0 .$

As we are working under the assumption $b > 0$, this condition can only be satisfied when $\beta > 0$, i.e, when the insulator is <u>topological</u>. The constant 'a' is determined from the square-integrability condition of the solution

$$\int_0^\infty |u^L(x)|^2 \, dx = 1 .$$

Then the full two-component zero-mode solution reads as

$$|\psi_0^L\rangle = u^L(x) \begin{pmatrix} 1 \\ i \end{pmatrix} .$$

How about the solution that is an eigenstate of $P = \sigma_y$ with eigenvalue -1. Identical steps lead to

$$\lambda_\pm^R = \left(-v_F \pm \sqrt{v_F^2 - 4b\beta}\right)/2b$$

For $\beta > 0$ and $b > 0$ the solution of the form

$$u(x) = a\, e^{-\lambda_+ x} + b\, e^{-\lambda_- x}$$

is not normalizable when $x \to +\infty$ as $\mathrm{Re}(\lambda_\pm) < 0$. Hence, the solution with $+1$ eigenvalue of $P = \sigma_y$ is the only normalizable zero mode when QSAHI occupy the semi-infinite region $0 \leq x < \infty$. The effective Hamiltonian for the 1D edge mode is now obtained by computing the matrix element of $H(k_y) = (v_F k_y)\sigma_y$ in the subspace of zero energy mode, yielding

$$H^L_{edge}(k_y) = \langle \psi^L_0 | H(k_y) | \psi^L_0 \rangle$$

$$\Rightarrow H^L_{edge}(k_y) = \left(2|u(x)|^2\right)(v_F k_y).$$

The solution with -1 eigenvalue of $P = \sigma_y$, on the other hand, is normalizable when the QSAHI occupy a semi-infinite region $-\infty < x \leq 0$, as shown in Fig. 14. The zero-energy mode then takes the form

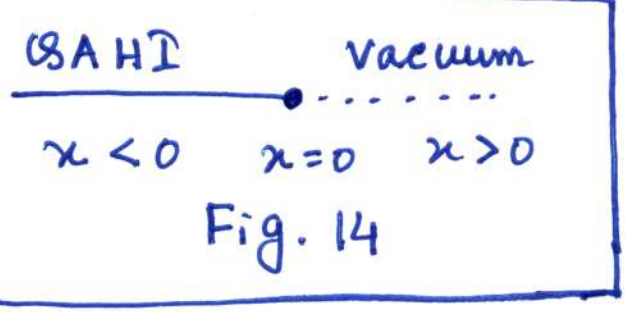

Fig. 14

$$|\psi^R_0\rangle = u^R(x) \begin{pmatrix} 1 \\ -i \end{pmatrix}$$

with the form of $u^R(x) = a\left(e^{-\lambda^R_+ x} - e^{-\lambda^R_- x}\right)$

The effective Hamiltonian for the edge mode is

$$H^{R}_{edge} = \langle \psi_0^R | H(k_y) | \psi_0^R \rangle = (2|u(x)|^2)(-v_F k_y)$$

Therefore the edge modes on the left and right edges propagate in the opposite direction, which is consistent with Fig. 12. The edge band structure is now shown in Fig. 15. The same calculation can now be repeated with semi-infinite extension in the y direction and with k_x as good quantum number. Note that the localization lengths of the zero mode $(\lambda^{L}_{\pm})^{-1}$ and $(\lambda^{R}_{\pm})^{-1}$ diverges as we approach the TQCP ($\beta = 0$) from the topological insulator side. Under this circumstance the chiral edge modes from the opposite ends of the system start to hybridize. At the TQCP $\beta = 0$, these modes are completely delocalized, hybridize and gap out following the principle of level repulsion. And in the trivial insulating phase there is edge mode : Bulk-boundary correspondence.

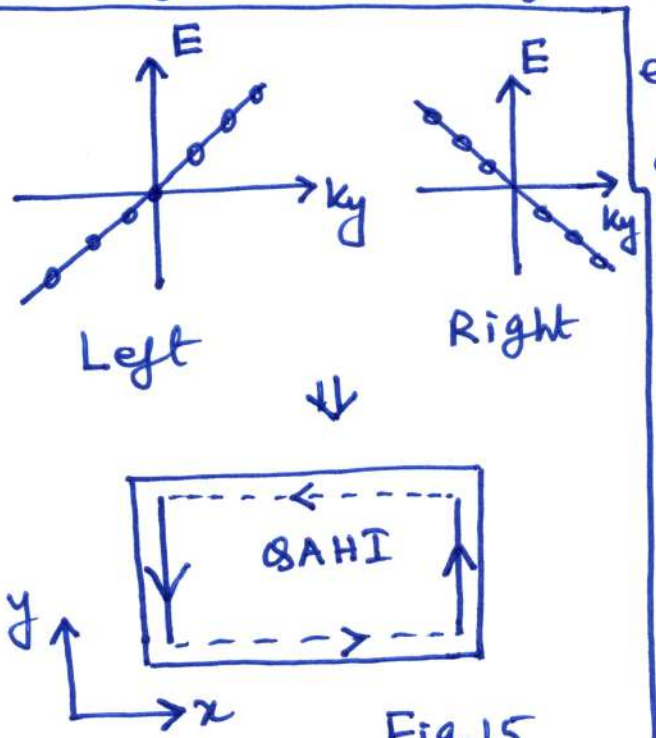

Fig. 15

A lattice model for QAHI:

So far we have discussed the model Hamiltonian for QAHI in the continuum limit. We started our discussion from massless Dirac fermions, realizable on honeycomb lattice & the added a mass term, proportional to $\beta\sigma_3$. We have shown that when such a mass term is accompanied by higher-gradient term like bk^2 then depending on the relative sign of β and b, the underlying insulator can be either topological or trivial. But the model Hamiltonian we discussed for QAHI is a universal one and doesn't depend on the underlying lattice structure. So, we now proceed to present a lattice regularized model for QAHI on square lattice by making the following substitution:

$k_x \longrightarrow \sin k_x$, $k_y \longrightarrow \sin k_y$. $\beta - bk^2 \rightarrow m_0 + t_0(\cos k_x + \cos k_y)$.

For simplicity we set the lattice spacing $a = 1$ & k_js should be recognized as $k_j a$. So, the model Hamiltonian now looks like

$$H_{lat} = t\left[\sin(k_x a)\sigma_x + \sin(k_y a)\sigma_y\right] + \left[m_0 + t_0(\cos k_x a + \cos k_y a)\right]\sigma_z$$

Note that the mass term (proportional to σ_z) vanishes at $m_0/t_0 = -2, 0, +2$. Here, t and t_0 are nearest-neighbor hopping amplitudes and m_0 is the on-site staggered potential.

The BZ of the square lattice is also square lattice in the momentum space, that features 4 time-reversal invariant momentum (TRIM) points:

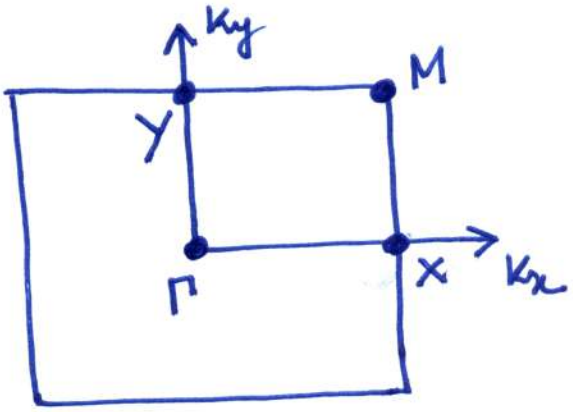

Fig. 16.

$\Gamma = (0,0)$, $M = \left(\frac{\pi}{a}, \frac{\pi}{a}\right)$, $X = (\pi/a, 0)$ & $Y = (0, \pi/a)$.

But X & Y are connected by C_4 symmetry, as shown in Fig. 16. Note that the Dirac kinetic term (lattice regularized), proportional to t vanishes at all 4 TRIM points. The band gap closes for the following values of m_0/t_0 and at the following TRIM points:

(a) $m_0/t_0 = -2$ at the Γ point

(b) $m_0/t_0 = 0$ at the X and Y points

(c) $m_0/t_0 = +2$ at the M point.

Now you can repeat the whole calculation, we did so far with only difference that momentum integral

$$\int_0^{2\pi} \int_0^{\infty} \frac{k\,dk\,d\phi}{(2\pi)^2} \longrightarrow \int_{-\pi/a}^{\pi/a} dk_x \int_{-\pi/a}^{\pi/a} dk_y \,,$$ yielding the following phase diagram:

Fig. 17:

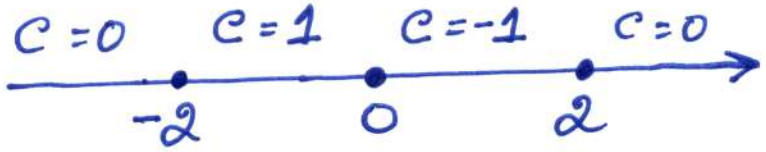

The phase diagram features two topological insulators with chern number $C = +1$ and $C = -1$ with a band gap closing in between them as they cannot be smoothly deformed into each other. These two topological insulators are separated from two trivial insulators by band gap closing.

Now, the question is what is the difference between two topological insulators with $C = +1$ and $C = -1$ respectively realized for $-2 < m_0/t_0 < 0$ and $0 < m_0/t_0 < 2$ since previously we have shown that the chern number is the momentum space skyrmion or anti-skyrmion number.

To see this connection we first focus in the parameter regime $-2 < m_0/t_0 < 0$ & expand H_{lat} around the $\Gamma = (0,0)$ point to arrive at an effective continuum model

$$H^{\Gamma}_{con} = ta(k_x \sigma_x + k_y \sigma_y) + \left[(m_0 + 2t_0) - \frac{t_0 a^2}{2} k^2\right]\sigma_z$$

define: $ta = v_F$, $m_0 = -2t_0 + \beta$, $\frac{t_0 a^2}{2} = b$.

$\Rightarrow \beta > 0$

$$\Rightarrow H^{\Gamma}_{con} = v_F(k_x \sigma_x + k_y \sigma_y) + (\beta - b k^2)\sigma_z.$$

which corresponds to our old model, featuring a momentum space skyrmion, centered around the Γ point with $C = +1$.

Next we expand the same lattice Hamiltonian around the M point in terms of $q_x = \pi/a - k_x$ & $q_y = \pi/a - k_y$ within the parameter regime $0 < m_0/t_0 < 2$, yielding a continuum model

$$H^{M}_{con} = ta(q_x \sigma_x + q_y \sigma_y) + \left[(m_0 - 2t_0) + \frac{t_0 a^2}{2}(q_x^2 + q_y^2)\right] \sigma_z .$$

define: $ta = v_F$, $m_0 = 2t_0 - \beta$, $\frac{t_0 a^2}{2} = b$.

$\Rightarrow \beta > 0$

$$\Rightarrow H^{M}_{con} = v_F(q_x \sigma_x + q_y \sigma_y) - (\beta - b q^2)\sigma_z$$

which corresponds to our old model, featuring a momentum space anti-skyrmion, centered around the M point with $C = -1$.

Therefore, we have realized that in a lattice regularized model we can find distinct topological phase with different topological invariants that feature band inversion around distinct TRIM point in the BZ. This possibility arises solely because lattice ~~short~~ has translational symmetry, yielding BZ with a number of TRIM points. Although these phases have distinct invariants they both support chiral edge modes. The question is what is the smoking gun probe to distinguish these phases?